Codon-Dependent tRNA Fluctuations Monitored with Fluorescence Polarization

Padmaja P. Mishra, Mohd Tanvir Qureshi, Wenhui Ren, and Tae-Hee Lee*
Department of Chemistry, The Pennsylvania State University, University Park, Pennsylvania

ABSTRACT During protein synthesis dictated by the codon sequence of messenger RNA, the ribosome selects aminoacyl-tRNA (aa-tRNA) with high accuracy, the exact mechanism of which remains elusive. By using a single-molecule fluorescence resonance energy transfer method coupled with fluorescence emission anisotropy, we provide evidence of random thermal motion of tRNAs within the ribosome in nanosecond timescale that we refer to as fluctuations. Our results indicate that cognate aa-tRNA fluctuates less frequently than near-cognate. This is counterintuitive because cognate aa-tRNA is expected to fluctuate more frequently to reach the ribosomal A-site faster than near-cognate. In addition, cognate aa-tRNA occupies the same position in the ribosome as near-cognate. These results argue for a mechanism which guides cognate aa-tRNA more accurately toward the A-site as compared to near-cognate. We suggest that a basis for this mechanism is the induced fit of the 30S subunit upon cognate aa-tRNA binding. Our single-molecule fluorescence resonance energy transfer time traces also point to a mechanistic model for GTP hydrolysis on elongation factor Tu mediated by aa-tRNA.

INTRODUCTION

The ribosome, a two-subunit (50S and 30S in prokaryotes) complex of RNAs and proteins, translates the nucleotide sequence of messenger ribonucleic acids (mRNA) into the amino-acid sequence of the respective proteins (1–5). The ribosome must select a series of aminoacyl transfer ribonucleic acids (aa-tRNAs) with an anticodon that can form Watson-Crick basepairs with the three-nucleotide sequence codon of mRNA designating each amino-acid residue. The accuracy of the aa-tRNA selection by the ribosome is extraordinarily high (10^{-4} error frequency), far beyond the thermodynamic limit (6). The delivery of aa-tRNA to the ribosome is mediated by a GTPase elongation factor Tu (EF-Tu) (7–9). A ternary complex of aa-tRNA, GTP, and EF-Tu interacts with the ribosome and mRNA (10–13). Upon correct anticodon-codon pairing between the aa-tRNA and mRNA, GTP is hydrolyzed on EF-Tu, and EF-Tu undergoes a conformational change that results in the dissociation of EF-Tu from the ribosome (2,7,14). This is followed by a proofreading step where an incorrectly selected aa-tRNA can be rejected (1,2). A nonhydrolyzable GTP analog, GDPNP, has been utilized to study the GTP hydrolysis process on EF-Tu by stalling the ribosome complex at an intermediate state (GTPase-activated state). However, the precise mechanism of how GTP hydrolysis effects EF-Tu dissociation from the ribosome remains elusive (7,15,16).

One of the key elements in the high efficiency aa-tRNA selection by the ribosome is the induced fit of the 30S ribosomal subunit upon binding of cognate aa-tRNA (16–18). Tighter binding of cognate aa-tRNA in a closed form of the 30S ribosomal subunit was proposed as a mechanism for the high efficiency aa-tRNA selection (16,17). In combination with the induced fit, fluctuations of aa-tRNA has also been proposed as an important element in the mechanism (16). Fluctuation in this report refers to the random thermal motion experienced by the aa-tRNA once it is loaded into the A-site. The motion is likely restricted rotational diffusion hinged at the anticodon stem loop (ASL) region within the 30S subunit of the ribosome. Typical rotational diffusion timescales of macromolecules in solution is in the range of hundreds of ps to a few ns, depending on the size and extent of intermolecular interactions (19). In contrast to these fluctuations, stochastic transitions of tRNA between different states are referred to as excursions from one state to another. These excursions occur in the timescale of a few to tens of ms (16). A fluctuating cognate aa-tRNA at the initial binding state is thought to reach the next intermediate state (A/T state) more frequently because the induced-fit positions cognate aa-tRNA more favorably toward the intermediate binding sites than near-cognate (16). However, there remains an absence of experimental evidence of tRNA fluctuations or how the fluctuations differ between cognate and near-cognate. This deficiency is mainly due to the time-resolution limit of the measurements.

The proposed mechanism of tRNA fluctuations contributing to the selection of tRNA (16) is well in line with a long-standing hypothesis suggesting that aa-tRNA delivers the information of codon-anticodon interactions in the 30S subunit to the 50S subunit and EF-Tu for subsequent GTP hydrolysis. Biochemical and structural studies provide strong support for this hypothesis (20–26). Recently, a structural study has suggested a potential channel for information flow via tRNA from the decoding site to the EF-Tu binding site (26). However, how this communication takes place

Submitted June 23, 2010, and accepted for publication October 18, 2010.

*Correspondence: txl18@psu.edu

Editor: Samuel Butcher.

0006-3495/10/12/3849/10 $2.00

doi: 10.1016/j.bpj.2010.10.026

through tRNA remains largely unknown. In this report, we begin to address this question by monitoring the codon-dependent fluctuations of tRNA and how the fluctuations contribute to the codon-dependent GTP hydrolysis in EF-Tu leading to the selection of the cognate aa-tRNA.

Fluorescence resonance energy transfer (FRET) is a valuable tool to monitor dynamic motions of molecules in the timescale of ms or longer (27–31). Some single molecule FRET methods to monitor structural or positional dynamics in a faster timescale (nanoseconds to approximately microseconds) are also available (32–34). These methods utilize either correlation method or the FRET efficiency distribution deconvolved from noise and dye photophysics as the measure of the timescale of a motion. However, collecting fluorescence photons for reliable correlation analysis in the timescale of microseconds or shorter, and the accurate measurements of noise and dye photophysics often require a laborious effort. These methods become particularly impractical when the system involves multiple complex molecules and assemblies of which purities and activities are far from 100% (because the method is implemented typically in a confocal geometry and allows the measurements of only one molecule at a time). Wide-field fluorescence methods with surface-immobilized molecules are preferred to study such a complex system.

Fluorescence emission anisotropy has long been employed to measure the rotational diffusion timescale of a biological molecule (19,35–37). When the entire molecule has much slower rotational motion compared to the local structural motions of interest, it is possible to utilize the FRET acceptor fluorescence emission anisotropy to determine how flexible the two fluorophores are, relative to each other. The fluorescence emission anisotropy of a FRET acceptor reflects the flexibility of the donor-labeled part, the acceptor-labeled part, and the link between the two fluorophores (33,38,39). In an intermolecular FRET system, the anisotropy can reflect the positional stability of the acceptor-labeled molecule with respect to the donor-labeled molecule. The timescale of the rotational diffusion that can be measured with this scheme is approximately in the range of nanoseconds, the fluorescence lifetime of the fluorophores.

Restricted free rotation of a fluorophore is a prerequisite of the scheme. It has been reported that the free rotation of cyanine dyes labeled at DNA is often restricted because the dyes stack well with nucleobases most likely through π-π interactions (40,41). In this study, we labeled tRNA with cyanine dyes at nucleobases through a 7~10 atom linker, which is long enough to allow the same type of π-π stacking interaction between the nucleobases and the cyanine dye. The validity of restricted free rotation of a fluorophore labeled at tRNA has been proven, as there is a significant difference in the anisotropy between a free dye and a dye labeled at free tRNA or between a dye at free tRNA and a dye at tRNA inside the ribosome (42).

Here, we demonstrate that FRET acceptor anisotropy can reflect structural flexibility of nucleic acid molecules. We applied the technique to observe the nanosecond fluctuation (i.e., random thermal motion) of aa-tRNA at an intermediate state during tRNA selection by the ribosome. To the best of our knowledge, this is the first direct evidence of tRNA fluctuations inside the ribosome, and our observation revealed that the fluctuation is codon-dependent. We also suggest a mechanism of the GTP hydrolysis on EF-Tu based on the observed single molecule FRET time traces.

MATERIALS AND METHODS

Instrumental setup

Our instrumental setup is shown in Fig. S1. A home-built microscope based on Nikon TE2000 with a 60× water immersion objective (Plan Apo; Nikon, Tokyo, Japan) was used to collect the single molecule fluorescence intensity data. FRET time traces were recorded with an electron multiplying charge-coupled device camera (iXon+ 897; Andor Technology, Belfast, UK) with image integration time of 35 ms. Fluorophores were excited in a total internal reflection geometry with a 532-nm solid state laser (Laser Quantum, Cheshire, UK). Cy5 emission is separated from Cy3 emission with a 650-nm dichroic mirror (650DCXL; Chroma Technology, Brattleboro, VT).

Bleedthrough of Cy3 emission to the Cy5 channel is typically <5% of Cy3 emission, and is subtracted from Cy5 emission during data analysis. Cy5 photobleaches before Cy3 does in most FRET pairs, and the bleedthrough rate of a Cy3 in a FRET pair can be determined by measuring the Cy3 intensity in the Cy5 channel after the Cy5 is photobleached. Direct excitation of Cy5 by the laser is negligible (typically <1% of total Cy5 emission at 0.5 FRET level). Microscope quartz slides were silanized and functionalized with polyethylene glycol (and biotinylated polyethylene glycol) before attaching the samples through biotin-streptavidin conjugation. Quartz surfaces were passivated with bovine serum albumin before the sample attachment. To measure the fluorescence decay rate of Cy3 and Cy5, a fluorimeter (FluoroMax-4; Horiva Jobin Yvon, Edison, NJ) with a pulsed diode laser at 560 nm (1.4 ns pulse, full width at half-maximum) or 650 nm (200 ps pulse, full width at half-maximum) was used.

For Cy3 fluorescence decay measurement, a DNA duplex without Cy5 was used. Sample buffer contains 10 mM Tris pH 8.0 and 100 mM NaCl. Fluorescence imaging buffer has 0.4% glucose and glucose oxidase/catalase mixture (0.16:2.6 units/μL) in addition to the sample buffer. Chemicals were purchased from Sigma Aldrich (St. Louis, MO), and the DNAs were custom-synthesized by Integrated DNA Technologies (Coralville, IA).

DNA, ribosome, mRNA, tRNA, and elongation factor Tu preparation

Labeled DNA used in the experiments was purchased from Integrated DNA Technologies. Materials for the aa-tRNA fluctuation measurements were prepared as published (16,42). Briefly, 70S ribosome was purified from *Escherichia coli* pKK3535 by a sucrose gradient technique. The S-100 portion of the cell extract was further purified to obtain enzymes to charge tRNA. The $tRNA^{fMet}$ was labeled with Cy3-maleimide at the s^4U8 position and $tRNA^{Phe}$ was labeled with Cy5-NHS ester at the acp^3U47 position (16). Messenger RNA was purchased from Thermo Scientific Dharmacon (Lafayette, CO) and has the codon sequence of

AUG UUU AAA CGU AAA UCU ACU

or

AUG CUU AAA CGU AAA UCU ACU,

which corresponds to fMet-Phe… or fMet-Leu…, respectively, for cognate or near-cognate. The 5′ end of mRNA is labeled with a biotin, which is utilized to immobilize the ribosome complex on a microscope slide surface. The 70S ribosomal particle, mRNA, and the initiator fMET-tRNA^{fMet} were incubated in the presence of the initiation factors (IF-1, IF-2, and IF-3) to form the initiated ribosome complex. Elongation factor Tu (EF-Tu) was purified as described (16). Phe-tRNA^{Phe} was complexed with EF-Tu and GDPNP, a nonhydrolyzable GTP analog. The ternary complex was incubated with the surface-attached ribosome for 10 min at room temperature before rinsing with the imaging buffer followed by FRET imaging. The buffer used for the tRNA fluctuation measurements contains 5 mM potassium phosphate pH 7.5, 90 mM potassium chloride, 0.5 mM calcium acetate, 5 mM ammonium acetate, 15 mM magnesium acetate, 1 mM DTT, 8 mM putrecine, 1 mM spermidine, and 0.4% glucose. Imaging buffer contains a glucose oxidase/catalase mixture (0.16/2.6 units/μL) in addition. An in-house developed hidden Markov model (HMM) algorithm was used to analyze the dynamics of the GTPase-activated state of the aa-tRNA/EF-Tu/GDPNP ternary complex inside the ribosome (43). More detailed rate constant analysis scheme is described in the Supporting Material.

RESULTS AND DISCUSSIONS

Method verification with DNA duplexes

Two requirements must be met to measure the structural flexibility of a molecule based on the FRET acceptor emission anisotropy: 1), the fluorophore labeled at a molecule must not rotate freely; and 2), the fluorescence decay time of the FRET acceptor must not be much shorter than the rotational diffusion time of the molecule. A Cy3-Cy5 pair labeled at a surface-immobilized DNA duplex meets these conditions because these dyes stack with nucleobases of DNA to inhibit their free rotation (40,41) and the fluorescence decay times of Cy5 are on the order of only a few hundred to a few nanoseconds.

A formula to estimate a timescale of the local motion between a FRET pair based on the fluorescence polarization of a FRET acceptor is presented here. The two major approximations made in the following equations are 1), that emission dipoles of the dyes are parallel to their absorption dipoles; and 2), that anisotropy decay can be described as a single exponential decay. The first approximation would not discount the validity of internal comparison between systems with the same fluorophores. A thorough description of the anisotropy decay behavior of a charged macromolecule (e.g., DNA) in an aqueous buffer solution would require impractically laborious modeling and analyses. Nonetheless, the single exponential decay time constant would be sufficient to compare the rotational freedom between structurally similar molecules in an identical environment. The main purpose of the presented quantitative description is to show how the acceptor emission anisotropy depends on FRET decay time, structural flexibility of the various parts of the molecule, and the acceptor fluorescence decay time.

Given a FRET pair in which the donor moves far more slowly than the acceptor, the acceptor fluorescence polarization (P) can be approximated to

$$\begin{aligned} P &= \frac{I_{a,\parallel} - I_{a,\perp}}{I_{a,\parallel} + I_{a,\perp}} \\ &= \frac{1}{2}\int_0^\infty k_f e^{-k_f t'} e^{-k_{Ra} t'} \int_0^\infty k_a e^{-k_a t} e^{-k_{Ra} t} dt dt' \\ &= \frac{1}{2}\frac{k_f}{k_f + k_{Ra}} \cdot \frac{k_a}{k_a + k_{Ra}}, \end{aligned} \tag{1}$$

where I_a is the acceptor fluorescence intensity (parallely or perpendicularly polarized according to the subscripts), k_f is fluorescence resonance energy transfer rate, k_{Ra} is the rotational decay rate of the acceptor convolved into the tumbling of the entire molecule, and k_a is acceptor fluorescence decay rate. Detailed derivation of the equation is included in the Supporting Material. When the entire molecule is fixed on a surface or moves more slowly as compared to the acceptor, the equation becomes

$$P = \frac{1}{2}\frac{k_f}{k_f + k_{ra}} \cdot \frac{k_a}{k_a + k_{ra}}, \tag{2}$$

where k_{ra} is the rotational decay rate of the acceptor.

The FRET rate (k_f) can be estimated from the fluorescence lifetime of the donor ($k_{d,fluorescent}$), FRET efficiency, and the quantum efficiency of the donor (Φ_d). Therefore, when the entire molecule and the donor have a restricted motion, the acceptor fluorescence polarization becomes dependent only on the acceptor rotational diffusion provided that the FRET decay rate and the acceptor fluorescence decay rate are constants:

$$FRET = \frac{k_f}{k_f + k_{d,fluorescent} + k_{a,non-fluorescent}}, \tag{3}$$

$$\Phi_d = \frac{k_{d,fluorescent}}{k_{d,fluorescent} + k_{d,non-fluorescent}}. \tag{4}$$

The fluorescence decay rate of the donor ($k_{d,fluorescent}$) can be determined from an ensemble measurement in the absence of the acceptor. The fluorescence decay rate of the acceptor (k_a) can be obtained from the ensemble lifetime of the acceptor emission in the presence of the donor.

Two sets of test measurements were made to evaluate the method. First, three DNA duplexes were assembled as shown in Fig. 1. The Cy3 dye position and the single-strand length were adjusted to yield varying structural flexibilities of the Cy5-labeled part or the link between the two dyes with a fixed FRET efficiency. Resulting fluorescence polarization values (0.45, 0.24, and 0.22 for the three duplexes) confirm that the fluorescence polarization of the FRET acceptor reflects the structural flexibility of the acceptor-labeled part or the link between the FRET pair. Subpopulations showing abnormal FRET (i.e., when the stable FRET value is <0.3 or >0.7) were ignored and were not included in the histograms. With fluorescence decay times obtained from ensemble measurements, we can deduce k_{ra} of the samples to estimate the timescale of the rotational diffusion of the single-strand linkers.

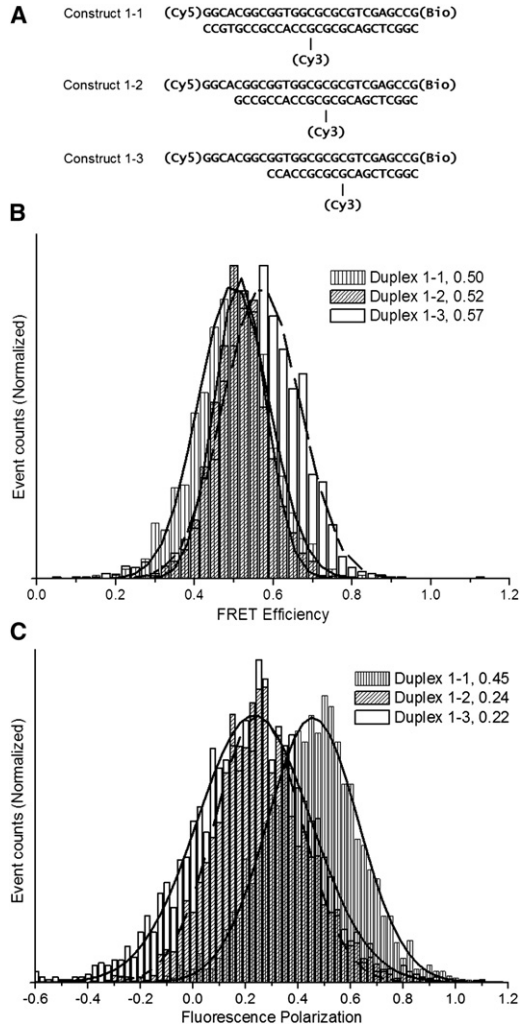

FIGURE 1 FRET and fluorescence polarization histograms obtained from DNA duplexes. (*A*) DNA duplexes 1-1, 1-2, and 1-3 used for the measurements. (*B*) FRET histograms of the three duplexes shown in panel *A* (at least 50 DNA duplexes per case). Values in the legend are the average FRET efficiencies obtained from Gaussian fittings. (*C*) Fluorescence polarization histograms of the three duplexes shown in panel *B*. Values in the legend are the average fluorescence polarizations obtained from Gaussian fittings.

Based on Eq. 2, we found that $1/k_{ra}$ for the three DNA duplexes in Fig. 1 are 7.8 ns, 0.97 ns, and 0.84 ns, respectively, for the duplexes 1-1, 1-2, and 1-3. Values used are $\Phi_d = 0.28$ (averaged from (44)), $\Phi_a \approx \Phi_d$ (according to our observation on the samples, the total fluorescence intensity stays approximately constant after photobleaching within <5% of the total fluorescence level), $1/k_{d,fluorescent} = 1.30$ ns (measured in an ensemble setup with duplex 1), and $1/k_a = 0.67$ ns (measured in a fluorometer with duplex 1). The fluorescence polarization value of the duplex 1-1 (= 0.45) that is close to the maximum possible value (= 0.5) indicates negligible tumbling of the entire molecule within the timescale of linker diffusion. Therefore, the fluorescence depolarization from the samples is mainly due to the motion of the flexible linker between the FRET pair and the timescale of the motion is in the order of nanoseconds.

To rule out the possibility that different polarization levels in Fig. 1 might derive from different rotational diffusion rates of entire DNA molecules due to their different weights, fluorescence polarization of another set of three DNA duplexes with similar weights were evaluated (Fig. 2). The fluorescence polarization of the three DNA duplexes in the control are 0.43, 0.22, and 0.19 for duplexes 2-1, 2-2, and 2-3, respectively. The rotational diffusion rate of the entire molecule of duplex 2-1 must be highest among the three constructs because it has the longest flexible region at the surface immobilized biotin end. However, the duplex 2-1 shows the highest emission polarization that is close to

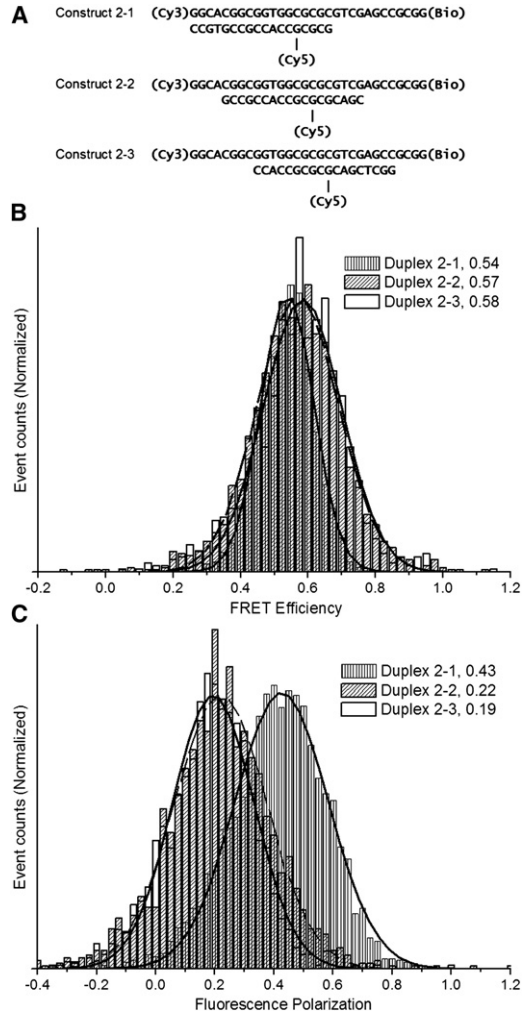

FIGURE 2 FRET and fluorescence polarization histograms obtained from a control set of DNA duplexes. (*A*) Control DNA duplexes 2-1, 2-2, and 2-3 used for the measurements. (*B*) FRET histograms of the three duplexes shown in panel *A* (at least 50 DNA duplexes per case). Values in the legend are the average FRET efficiencies obtained from Gaussian fittings. (*C*) Fluorescence polarization histograms of the three duplexes shown in panel *B*. Values in the legend are the average fluorescence polarizations obtained from Gaussian fittings.

the maximum possible value (= 0.50), indicating that the rotational diffusion of the entire construct is too slow to contribute to the depolarization. We conclude that the local motion between a FRET pair accounts for most of the observed depolarization. Therefore, the acceptor emission polarization can be used as a measure of the local structural flexibility between a FRET pair positioned within the same complex (e.g., double-stranded DNA) or between two complexes (e.g., intermolecular system of tRNAs in the ribosome).

Although a more rigorous modeling and quantitative analysis is necessary to obtain accurate values for rotational diffusion timescales and to determine the precise physical meaning of the fluorescence depolarization rate, it is evident that a lower rotational rate and a high fluorescence polarization can be interpreted as less flexible and more restricted motion. Therefore, this simple method and analysis is sufficient for internal comparison between systems with varying degrees of local motion or positional stabilities. As a means to better understand how tRNAs are correctly selected by the ribosome, we employed this method to assess the fluctuations of cognate and near-cognate aa-tRNA inside the ribosome.

Fluctuations of cognate and near-cognate aa-tRNA at an intermediate state during tRNA selection by the ribosome

The ribosome complex with mRNA and a peptidyl tRNA labeled with Cy3 shows three FRET efficiencies during the selection of aa-tRNA labeled with Cy5 (Fig. 3 *A*) (16,42). The three FRET efficiencies are 0.2~0.3 (low-FRET), 0.4~0.5 (mid-FRET), and >0.7 (high-FRET) for the initial binding of the aa-tRNA/EF-Tu/GTP ternary complex to the ribosome, GTPase activation/GTP hydrolysis on EF-Tu (aa-tRNA in the A/T state), and the full accommodation of the aa-tRNA to the ribosomal A-site, respectively (16,42). We used a nonhydrolyzable GTP analog, GDPNP, to stall the ternary complex of aa-tRNA/EF-Tu/GDPNP at the A/T state, yielding a long-living 0.4~0.5 FRET state (Fig. 3, *B–D*, and Fig. S2) (16).

Fig. 3 *B* shows typical fluorescence intensity traces collected by the setup shown in Fig. S1 and Fig. 3 *A*. The intensities of the two polarization components of Cy5 were summed up to yield the total Cy5 emission intensity (Fig. 3 *C*). The stalled mid-FRET state shows short excursions to the high-FRET state as demonstrated in Fig. 3 *D* (the three short excursions to the high-FRET state ~15 s). These excursions indicate that aa-tRNA at the A/T state attempts to reach the A-site before the GTP hydrolysis on EF-Tu(Fig. 4). Cognate aa-tRNA reaches the A-site 2.6-fold more frequently than near-cognate (Fig. 4 *B*). The rates in Fig. 4 *B* are the results of hidden Markov model analyses (43) with 100 complexes for cognate and 83 complexes for near-cognate. The FRET traces were

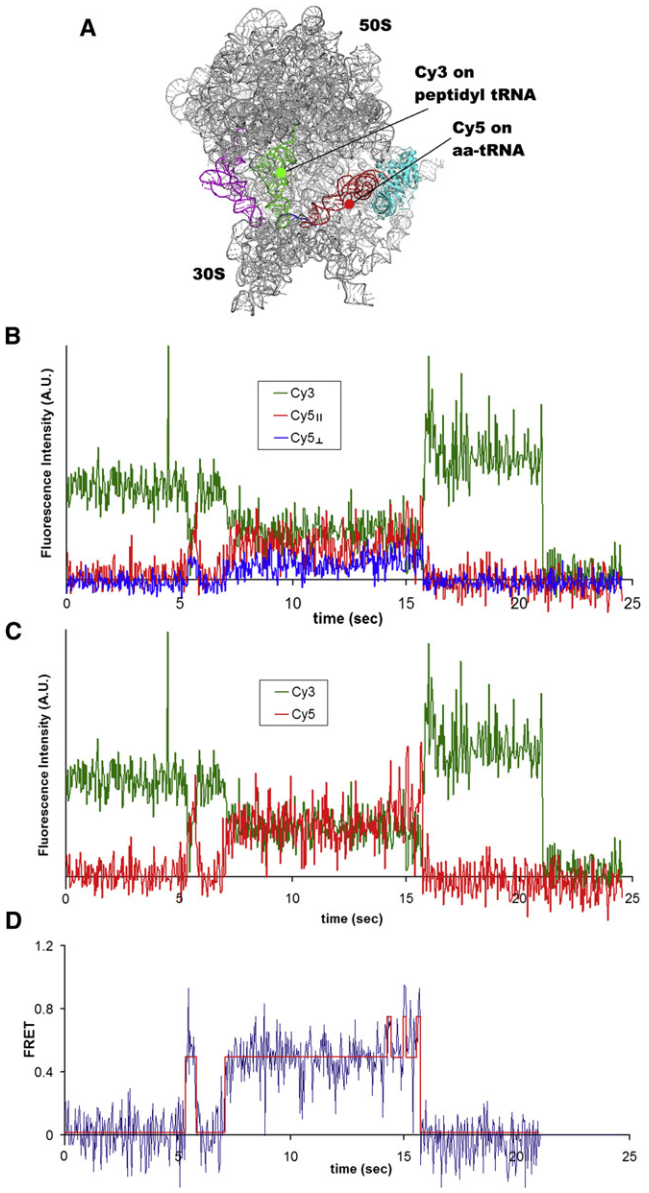

FIGURE 3 Experimental setup and a typical single molecule FRET and acceptor anisotropy result obtained from aa-tRNA/EF-Tu/GDPNP delivered to the ribosome using the anisotropy instrumental setup in Fig. S1. (*A*) The structure of the ribosome complex with the GTPase activated ternary complex. (*B*) Three fluorescence intensity time traces (*green*, Cy3; *red*, Cy5 parallel; and *orange*, Cy5 perpendicular) obtained from the setup in Fig. S1. (*C*) The same traces as in panel *B* with the two Cy5 traces summed up to yield the total Cy5 intensity trace (*red*). Cy3 intensity trace (*green*) is unchanged from panel *B*. (*D*) FRET efficiency trace calculated from the traces in panel *C*. Short excursions from the mid-FRET state to the high-FRET state are evident.

collected with a conventional two-color FRET setup to achieve a high data collection efficiency (a complete set of data is displayed as postsync plots in Fig. S2). It has been shown that the error of the HMM analysis with this amount of data is typically within 20% (43).

A three-panel FRET anisotropy setup (Fig. S1) was used to collect FRET signals. FRET efficiency histograms and the

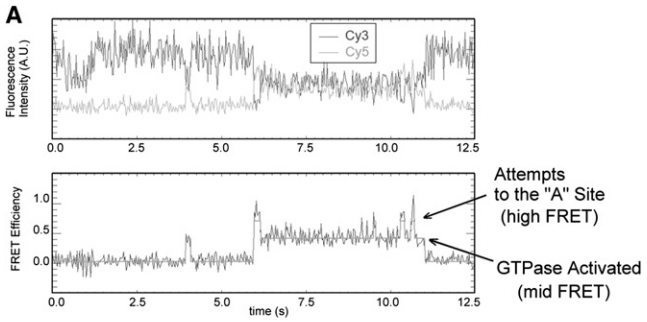

B

(rates, /s)

	mid-FRET → 0 (1/Lifetime of GTPase activated state)	mid-FRET →high-FRET (Sampling rate to the "A" site)	high-FRET →mid-FRET (1/Lifetime of transient "A" site sampling)
Cognate	0.12	1.55	4.4
Near-cognate	0.89	0.60	6.0

FIGURE 4 Summary of single molecule FRET results revealing the dynamics of the GTPase activated state. (*A*) A typical single molecule FRET trace of the stalled GTPase activated state (mid-FRET state) showing short excursions to the fully accommodated state (high-FRET state). (*B*) Rate constants in and out of the GTPase activated state were analyzed by an HMM algorithm (43). Traces from 72 and 97 ribosome particles were used for panels *A* and *B*, respectively. Detailed analysis scheme is described in the Supporting Material.

acceptor fluorescence polarization values of cognate (phe-tRNA^{phe} to UUU codon) and near-cognate (phe-tRNA^{phe} to CUU codon) at the GTPase-activated state (the A/T state) are shown (Fig. 5). The cognate and near-cognate at the A/T state have an identical FRET efficiency (0.43, Fig. 5 *A*). The same FRET efficiency suggests that the cognate and the near-cognate aa-tRNA in the A/T state occupy the same position in the ribosome. This is one fundamental difference between this study and the previous report (16) where the equilibrium position of the initially bound cognate aa-tRNA was slightly deeper inside the ribosome as compared to the near-cognate.

Fluorescence polarization values for the cognate and near-cognate aa-tRNAs are significantly different (Fig. 5 *B* and Fig. S3), as cognate is 0.288 ± 0.011 and near-cognate is 0.234 ± 0.003. Free Cy5, Cy5 labeled at free tRNA^{phe}, and Cy5 labeled at tRNA^{phe} inside the ribosome report anisotropy values of 0.14, 0.15, and 0.25, respectively (see Table 1 in the supporting information of (42)). The fluorescence decay times of Cy5 in the three cases are 0.845 ns, 1.20 ns, and 1.35 ns, respectively, which confirms that the dye is not freely rotating (Fig. 6). Therefore, the difference in the acceptor emission fluorescence polarization reflects the difference in the positional stability between the two aa-tRNA molecules. The higher fluorescence polarization for cognate aa-tRNA is consistent with less positional flexibility and more restricted fluctuations than observed for near-cognate aa-tRNA.

Crystal structures have suggested that the binding of cognate tRNA induces conformation changes of the 30S ribosomal subunit. This induced-fit mechanism was proposed as a basis of the high efficiency aa-tRNA selection

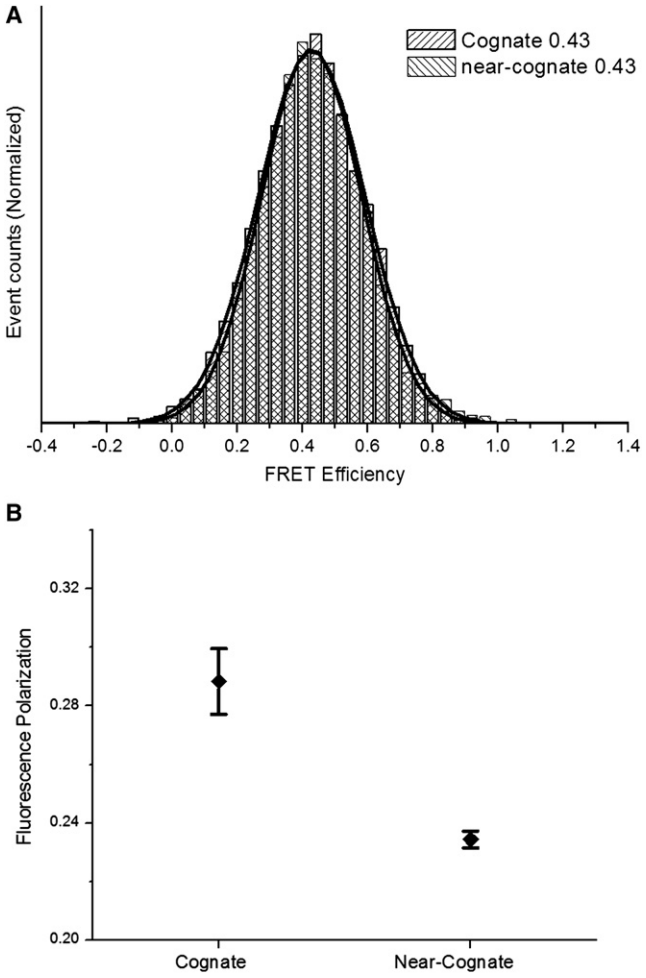

FIGURE 5 FRET histograms and fluorescence polarization values of the GTPase activated state with cognate and near-cognate complexes. Parts of traces with >1 s of stable mid-FRET state were taken into analysis. Traces from 48 and 53 ribosome particles were used for the cognate and near-cognate complexes, respectively. (*A*) FRET histograms of the GTPase activated state of a cognate aa-tRNA molecule and a near-cognate aa-tRNA molecule. Values in the legend are the average FRET efficiencies obtained from Gaussian fittings. (*B*) Average fluorescence polarizations and errors obtained from Gaussian fittings of fluorescence polarization histograms shown in Fig. S3.

by the ribosome (17). Previous single molecule results have shown that cognate aa-tRNA at the initial binding stage occupies a slightly deeper position inside the ribosome, which is likely a result of the induced fit (16). This favorable positioning of the cognate was proposed as a mechanism of accurate aa-tRNA selection. Although the report (16) proposed tRNA fluctuations as a major factor in determining the fidelity of translation, it did not provide any evidence of tRNA fluctuations.

In this study, we have not observed any difference in the position of aa-tRNA at the A/T state between the cognate and the near-cognate. In addition, we monitored the fluctuations of tRNA by fluorescence polarization and the results in Fig. 5 *B* indicate that the cognate aa-tRNA fluctuates less

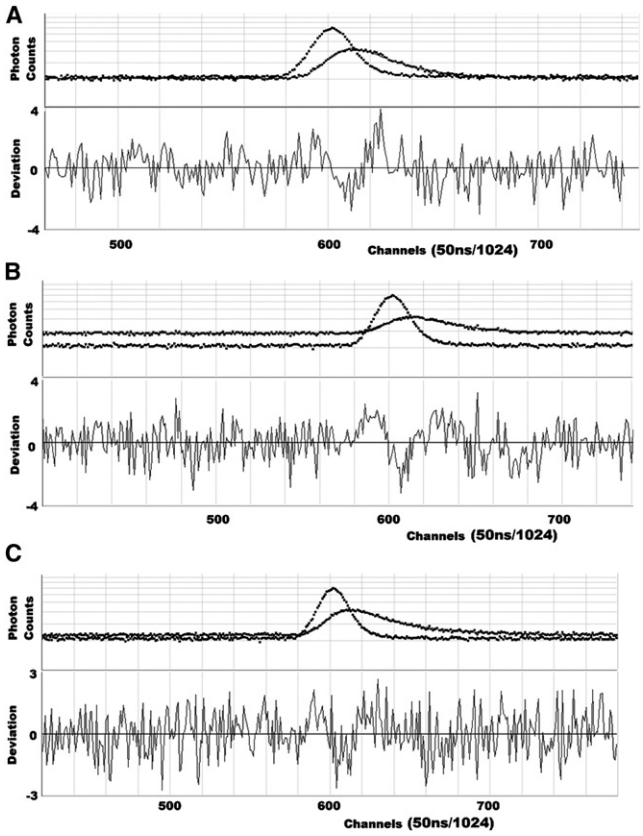

FIGURE 6 Fluorescence lifetime measurements report 0.845 ns, 1.20 ns, and 1.35 ns for free Cy5 (*A*), Cy5 labeled at phe-tRNA^{phe} (*B*), and Cy5 labeled at phe-tRNA^{phe} accommodated in the A-site of the ribosome (*C*), respectively. The peak photon count of the samples was 4200 and that of the instrumental response was 7000. Single exponential decay (*thin gray line*) convolved into the instrumental response (*black dots*) fits the fluorescence decay (*dark gray dots*) very well according to the residual of the fitting shown as deviation. The anisotropy values for cases *A–C* were reported as 0.14, 0.15, and 0.25, respectively (Table 1 of the supporting information in (42)). Therefore, free Cy5 has a higher freedom of rotation than Cy5 labeled at tRNA, which has a higher freedom of rotation than Cy5 labeled at tRNA inside the ribosome.

than the near-cognate. These results strongly suggest that there must be a mechanism that steers cognate aa-tRNA at the A/T state more accurately toward the A-site to account for the higher chance of cognate docking as compared to near-cognate. We suggest that the conformational changes in the 30S ribosomal subunit upon binding cognate aa-tRNA guides cognate aa-tRNA to the A-site. As a result, there is more restricted fluctuation of cognate aa-tRNA that biases its movement to the A-site. This is further supported by the observed 2.6-fold more frequent transient excursions to the A-site as compared to near-cognate (1.55 /s and 0.60 /s for cognate and near-cognate aa-tRNA, respectively; see Fig. 5 *B*). The excursions of aa-tRNA to the A-site before GTP hydrolysis on EF-Tu indicates that GTP hydrolysis is not required for aa-tRNA to move toward the A-site, which has also been observed and discussed (15,45).

So how might GTP hydrolysis on EF-Tu be regulated by cognate aa-tRNA binding? Based on our observations, we propose that the mechanical energy derived from the conformational changes experienced by the 30S subunit upon cognate binding is transmitted to EF-Tu to catalyze GTP hydrolysis. As EF-Tu is tightly bound to the ribosome, the observed transient motions of aa-tRNA to the A-site must cause mechanical tension in EF-Tu. This tension stems from the 30S subunit conformational changes which steer the aa-tRNA. This is supported by the crystal structure showing a larger conformational change in the 30S subunit upon cognate aa-tRNA binding as compared to near-cognate aa-tRNA (17) and the tighter binding to cognate aa-tRNA, evidenced as a longer dwell time inside the ribosome compared to near-cognate aa-tRNA (Fig. S2). These differences will yield a higher tension on EF-Tu upon cognate aa-tRNA binding as compared to near-cognate aa-tRNA binding, which can lead to preferential GTP hydrolysis on EF-Tu only upon cognate aa-tRNA binding. A possible hypothesis is that the mechanical tension transmitted through aa-tRNA induces a conformational change in EF-Tu resulting in GTP hydrolysis. Unlike previous models where GTP is somehow hydrolyzed preferably upon cognate binding before aa-tRNA reaches the A-site, our model explains how GTP hydrolysis occurs only when the cognate aa-tRNA accesses the A-site. Our results reveal that aa-tRNA attempts to reach the A-site before GTP hydrolysis and that cognate tRNAs make more frequent attempts than near-cognate, strongly supporting the proposed model.

Several reports have shown that parts of tRNA other than the anticodon play important roles in various steps of translation (20–22,46). Altered top basepairs in the anticodon helix (nt 27-43) displayed unusual coding behaviors (22,46). More recently, it was reported that full-length tRNA is necessary to trigger GTP hydrolysis (20,21). No rapid GTP hydrolysis was shown to take place when they used tRNA fragments (anticodon/D arm only or acceptor stem/T arm only) instead of full-length tRNAs. One of the two tRNA fragments formed contacts only with the 30S and the other one with the 50S subunit. Even in cases with drugs stabilizing the unfavorable coding situation from nonmatching basepairs in codon-anticodon interaction, no rapid GTP hydrolysis was observed.

These results strongly suggest that intact full tRNA is necessary to trigger GTPase activity of EF-Tu and subsequent GTP hydrolysis. There is also evidence of interaction between EF-Tu and the conserved 530 loop of 16S rRNA of 30S subunit (47). Structural studies (10,48–50) indicate that EF-Tu conformation changes upon GTP hydrolysis and yields much weaker interactions between EF-Tu and aa-tRNA. These results lend further support to our model, as it proposes that aa-tRNA energized by the ribosome structural changes transmits the mechanical tension from the anticodon to the acceptor stem region and forces

conformational changes in EF-Tu, resulting in the separation of the tRNA from EF-Tu.

Electron-microscopic studies revealed the complex conformational rearrangements of tRNA during the initial selection (23) and suggested that tRNA acts as a molecular spring during the course of an elongation cycle (24,25). With a virtually unchanged anticodon stem loop (ASL) position, the tRNA acceptor arm must move ~4.6 nm to be fully accommodated into the ribosome. Based on the length of tRNA (>7 nm), it is not difficult to imagine that slight mispositioning of tRNA in the decoding site (ASL region) can yield substantial differences in the acceptor arm position when fully accommodated. Some mutagenesis results also suggested that conformational changes in tRNA play a critical role in the induced-fit mechanism. Researchers found that single substitution in the D-arm of tRNA accelerate the miscoded tRNA selection (21). Another mutagenesis result suggested that tRNA self-catalyzes the peptide bond formation (51). A mutated P-site tRNA (or Peptidyl tRNA) yielded dramatically lower rates of peptide bond formation without compromising the binding efficiency.

Positioning of the ternary complex (EF-Tu/aa-tRNA/GTP) should be highly precise to form correct multiple contacts with the ribosome (L7/L12; GTPase-associated center (GAC); SH5; Sarcin-Ricin Loop (SRL) with the EF-Tu, LH69, and S12 with the tRNA acceptor stem; LH43 with the tRNA TψC loop; anticodon loop of tRNA; and decoding-site residues A1492, A1493, and G530 of small ribosomal subunit) (9,13,25,52–54). The contact formation has been found to be essential in the tRNA selection process. It has been shown that the changes in elements which contact the ternary complex directly (L7, L6, S12, SRL, and LH69) alter fidelity dramatically (15,55–58). For GTP hydrolysis on EF-Tu, the ternary complex should make proper contact with SRL and GAC (9,25,59). To make these contacts, the ternary complex should further move into the ribosome after the initial binding and codon-recognition. This movement is likely coupled to tRNA hinge motion due to the strong affinity between tRNA and EF-Tu. Therefore, it is reasonable to imagine that small differences in tRNA position at the ribosome decoding site can make a large difference in the chance of the ternary complex forming all the necessary contacts with the ribosome.

Our model requires differential tension in the tRNA molecule depending on the strength of codon-anticodon interaction. One factor for creating the tension is strong interaction between ASL of tRNA and mRNA/ribosome. Strong interactions among the acceptor stem of tRNA, EF-Tu, and the ribosome is another requirement for high tension on tRNAs. The above results and suggestions state that a cognate ternary complex has stronger interactions with the ribosome in both ends of the ternary complex (ASL and acceptor stem/EF-Tu). Consequently, a cognate ternary complex conveys a stronger tension through tRNA to the GTPase center of EF-Tu and GAC, as compared to near-cognate complexes.

Lastly, low Mg^{2+} ion concentration is known to cause more dynamic tRNA motion in the ribosome, likely due to higher intramolecular flexibility of tRNAs and weaker interactions between tRNAs and the ribosome (16,60,61). Therefore, we expect that the fluctuations of tRNAs becomes more important for correct tRNA selection because tight interactions between codon and anticodon is necessary for GTP hydrolysis and transmission of the mechanical tension through tRNA would be less efficient at lower Mg^{2+} ion concentrations. This is in good agreement with previous results that showed higher translation fidelity at a lower Mg^{2+} concentration (16).

CONCLUSIONS

We demonstrate a simple single molecule method to measure local structural flexibility of a macromolecular assembly or the positional stability of a macromolecule. We applied the method to probe the behavior of fluctuating aa-tRNA inside the ribosome. Our results indicate that aa-tRNA fluctuates inside the ribosome and cognate aa-tRNA fluctuates less than near-cognate. We propose that fluctuating cognate aa-tRNA is guided by the ribosome toward the A-site by the conformational changes in the 30S subunit. To the best of our knowledge, this is the first direct experimental evidence showing tRNA fluctuations in the ribosome and the first direct observation of how induced fit affects the ns dynamics of tRNA inside the ribosome. We also propose that a larger 30S subunit conformational change induced by cognate aa-tRNA may be a basis of preferential GTP hydrolysis on EF-Tu upon cognate binding.

SUPPORTING MATERIAL

Three figures, six equations, and one method are available at http://www.biophysj.org/biophysj/supplemental/S0006-3495(10)01314-7.

We thank Prof. Harry Noller (University of California at Santa Cruz) who provided us with the plasmid pKK3535 and Prof. Takuya Ueda (University of Tokyo, Tokyo, Japan) who provided us with the plasmids for the initiation factors IF-1, -2, and -3.

This work was supported by National Institutes of Health (grant No. GM0799601), Searle Scholar Award, and the Camillie and Henry Dreyfus New Faculty Award to T.L.

REFERENCES

1. Green, R., and H. F. Noller. 1997. Ribosomes and translation. *Annu. Rev. Biochem.* 66:679–716.
2. Rodnina, M. V., and W. Wintermeyer. 2001. Ribosome fidelity: tRNA discrimination, proofreading and induced fit. *Trends Biochem. Sci.* 26:124–130.
3. Ban, N., P. Nissen, …, T. A. Steitz. 2000. The complete atomic structure of the large ribosomal subunit at 2.4. Å resolution. *Science.* 289:902–921.

4. Yonath, A., C. Glotz, …, H. G. Wittmann. 1988. Characterization of crystals of small ribosomal subunits. *J. Mol. Biol.* 203:831–834.
5. Cate, J. H., M. M. Yusupov, …, H. F. Noller. 1999. X-ray crystal structures of 70S ribosome functional complexes. *Science.* 285:2095–2104.
6. Kurland, C. G., D. Hughes, and M. Ehrenberg. 1996. *In* Limitations of Translational Accuracy. ASM Press, Washington, DC.
7. Rodnina, M. V., R. Fricke, …, W. Wintermeyer. 1995. Codon-dependent conformational change of elongation factor Tu preceding GTP hydrolysis on the ribosome. *EMBO J.* 14:2613–2619.
8. Hunter, S. E., and L. L. Spremulli. 2004. Mutagenesis of glutamine 290 in *Escherichia coli* and mitochondrial elongation factor Tu affects interactions with mitochondrial aminoacyl-tRNAs and GTPase activity. *Biochemistry.* 43:6917–6927.
9. Moazed, D., J. M. Robertson, and H. F. Noller. 1988. Interaction of elongation factors EF-G and EF-Tu with a conserved loop in 23S RNA. *Nature.* 334:362–364.
10. Kjeldgaard, M., P. Nissen, …, J. Nyborg. 1993. The crystal structure of elongation factor EF-Tu from *Thermus aquaticus* in the GTP conformation. *Structure.* 1:35–50.
11. Abel, K., M. D. Yoder, …, F. Jurnak. 1996. An α to β conformational switch in EF-Tu. *Structure.* 4:1153–1159.
12. Stark, H., M. V. Rodnina, …, M. van Heel. 1997. Visualization of elongation factor Tu on the *Escherichia coli* ribosome. *Nature.* 389: 403–406.
13. Stark, H., M. V. Rodnina, …, M. van Heel. 2002. Ribosome interactions of aminoacyl-tRNA and elongation factor Tu in the codon-recognition complex. *Nat. Struct. Biol.* 9:849–854.
14. Rodnina, M. V., and W. Wintermeyer. 2001. Fidelity of aminoacyl-tRNA selection on the ribosome: kinetic and structural mechanisms. *Annu. Rev. Biochem.* 70:415–435.
15. Blanchard, S. C., R. L. Gonzalez, …, J. D. Puglisi. 2004. tRNA selection and kinetic proofreading in translation. *Nat. Struct. Mol. Biol.* 11:1008–1014.
16. Lee, T.-H., S. C. Blanchard, …, S. Chu. 2007. The role of fluctuations in tRNA selection by the ribosome. *Proc. Natl. Acad. Sci. USA.* 104:13661–13665.
17. Ogle, J. M., F. V. Murphy, …, V. Ramakrishnan. 2002. Selection of tRNA by the ribosome requires a transition from an open to a closed form. *Cell.* 111:721–732.
18. Adilakshmi, T., D. L. Bellur, and S. A. Woodson. 2008. Concurrent nucleation of 16S folding and induced fit in 30S ribosome assembly. *Nature.* 455:1268–1272.
19. Lakowicz, J. R. 2006. Principles of Fluorescence Spectroscopy. Springer, Berlin, Heidelberg.
20. Piepenburg, O., T. Pape, …, M. V. Rodnina. 2000. Intact aminoacyl-tRNA is required to trigger GTP hydrolysis by elongation factor Tu on the ribosome. *Biochemistry.* 39:1734–1738.
21. Cochella, L., and R. Green. 2005. An active role for tRNA in decoding beyond codon:anticodon pairing. *Science.* 308:1178–1180.
22. Schultz, D. W., and M. Yarus. 1994. tRNA structure and ribosomal function. II. Interaction between anticodon helix and other tRNA mutations. *J. Mol. Biol.* 235:1395–1405.
23. Schuette, J.-C., F. V. Murphy, 4th, …, C. M. Spahn. 2009. GTPase activation of elongation factor EF-Tu by the ribosome during decoding. *EMBO J.* 28:755–765.
24. Frank, J., J. Sengupta, …, M. Ehrenberg. 2005. The role of tRNA as a molecular spring in decoding, accommodation, and peptidyl transfer. *FEBS Lett.* 579:959–962.
25. Valle, M., A. Zavialov, …, J. Frank. 2003. Incorporation of aminoacyl-tRNA into the ribosome as seen by cryo-electron microscopy. *Nat. Struct. Biol.* 10:899–906.
26. Schmeing, T. M., R. M. Voorhees, …, V. Ramakrishnan. 2009. The crystal structure of the ribosome bound to EF-Tu and aminoacyl-tRNA. *Science.* 326:688–694.
27. Förster, T. 1959. Transfer mechanisms of electronic excitation. *Discuss. Faraday Soc.* 27:7–17.
28. Deniz, A. A., M. Dahan, …, P. G. Schultz. 1999. Single-pair fluorescence resonance energy transfer on freely diffusing molecules: observation of Förster distance dependence and subpopulations. *Proc. Natl. Acad. Sci. USA.* 96:3670–3675.
29. Ha, T., A. Y. Ting, …, S. Weiss. 1999. Temporal fluctuations of fluorescence resonance energy transfer between two dyes conjugated to a single protein. *Chem. Phys.* 247:107–118.
30. Zhuang, X., T. Ha, …, S. Chu. 2000. Fluorescence quenching: a tool for single-molecule protein-folding study. *Proc. Natl. Acad. Sci. USA.* 97:14241–14244.
31. Ha, T., I. Rasnik, …, S. Chu. 2002. Initiation and re-initiation of DNA unwinding by the *Escherichia coli* Rep helicase. *Nature.* 419:638–641.
32. Antonik, M., S. Felekyan, …, C. A. Seidel. 2006. Separating structural heterogeneities from stochastic variations in fluorescence resonance energy transfer distributions via photon distribution analysis. *J. Phys. Chem. B.* 110:6970–6978.
33. Kalinin, S., S. Felekyan, …, C. A. Seidel. 2007. Probability distribution analysis of single-molecule fluorescence anisotropy and resonance energy transfer. *J. Phys. Chem. B.* 111:10253–10262.
34. Lee, T.-H., L. J. Lapidus, …, S. Chu. 2007. Measuring the folding transition time of single RNA molecules. *Biophys. J.* 92:3275–3283.
35. Brochon, J.-C., P. Wahl, and J.-C. Auchet. 1974. Fluorescence time-resolved spectroscopy and fluorescence anisotropy decay of the *Staphylococcus aureus* endonuclease. *Eur. J. Biochem.* 41:577–583.
36. Harms, G. S., M. Sonnleitner, …, T. Schmidt. 1999. Single-molecule anisotropy imaging. *Biophys. J.* 77:2864–2870.
37. Kungl, A. J., N. V. Visser, …, M. Auer. 1998. Time-resolved fluorescence anisotropy of HIV-1 protease inhibitor complexes correlates with inhibitory activity. *Biochemistry.* 37:2778–2786.
38. Rasnik, I., S. A. McKinney, and T. Ha. 2005. Surfaces and orientations: much to FRET about? *Acc. Chem. Res.* 38:542–548.
39. Gopich, I., and A. Szabo. 2005. Theory of photon statistics in single-molecule Förster resonance energy transfer. *J. Chem. Phys.* 122:14707.
40. Armitage, B. A. 2005. Topics in Current Chemistry: Cyanine Dye—DNA Interactions: Intercalation, Groove Binding, and Aggregation. Springer, Berlin/Heidelberg.
41. Iqbal, A., L. Wang, …, D. G. Norman. 2008. The structure of cyanine 5 terminally attached to double-stranded DNA: implications for FRET studies. *Biochemistry.* 47:7857–7862.
42. Blanchard, S. C., H. D. Kim, …, S. Chu. 2004. tRNA dynamics on the ribosome during translation. *Proc. Natl. Acad. Sci. USA.* 101: 12893–12898.
43. Lee, T.-H. 2009. Extracting kinetics information from single-molecule fluorescence resonance energy transfer data using hidden Markov models. *J. Phys. Chem. B.* 113:11535–11542.
44. Harvey, B. J., C. Perez, and M. Levitus. 2009. DNA sequence-dependent enhancement of Cy3 fluorescence. *Photochem. Photobiol. Sci.* 8: 1105–1110.
45. Frank, Jr., J., and R. L. Gonzalez. 2010. Structure and dynamics of a processive Brownian motor: the translating ribosome. *Annu. Rev. Biochem.* 79:381–412.
46. Hirsh, D. 1971. Tryptophan transfer RNA as the UGA suppressor. *J. Mol. Biol.* 58:439–458.
47. Powers, T., and H. F. Noller. 1993. Evidence for functional interaction between elongation factor Tu and 16S ribosomal RNA. *Proc. Natl. Acad. Sci. USA.* 90:1364–1368.
48. Polekhina, G., S. Thirup, …, J. Nyborg. 1996. Helix unwinding in the effector region of elongation factor EF-Tu-GDP. *Structure.* 4: 1141–1151.
49. Nissen, P., M. Kjeldgaard, …, J. Nyborg. 1995. Crystal structure of the ternary complex of Phe-tRNAPhe, EF-Tu, and a GTP analog. *Science.* 270:1464–1472.

50. Berchtold, H., L. Reshetnikova, …, R. Hilgenfeld. 1993. Crystal structure of active elongation factor Tu reveals major domain rearrangements. *Nature.* 365:126–132.

51. Weinger, J. S., K. M. Parnell, …, S. A. Strobel. 2004. Substrate-assisted catalysis of peptide bond formation by the ribosome. *Nat. Struct. Mol. Biol.* 11:1101–1106.

52. Hausner, T. P., J. Atmadja, and K. H. Nierhaus. 1987. Evidence that the G2661 region of 23S rRNA is located at the ribosomal binding sites of both elongation factors. *Biochimie.* 69:911–923.

53. Vorstenbosch, E., T. Pape, …, W. Wintermeyer. 1996. The G222D mutation in elongation factor Tu inhibits the codon-induced conformational changes leading to GTPase activation on the ribosome. *EMBO J.* 15:6766–6774.

54. Ogle, J. M., D. E. Brodersen, …, V. Ramakrishnan. 2001. Recognition of cognate transfer RNA by the 30S ribosomal subunit. *Science.* 292:897–902.

55. Dey, D., A. V. Oleinikov, and R. R. Traut. 1995. The hinge region of *Escherichia coli* ribosomal protein L7/L12 is required for factor binding and GTP hydrolysis. *Biochimie.* 77:925–930.

56. Kühberger, R., W. Piepersberg, …, A. Böck. 1979. Alteration of ribosomal protein L6 in gentamicin-resistant strains of *Escherichia coli*. Effects on fidelity of protein synthesis. *Biochemistry.* 18:187–193.

57. Powers, T., and H. F. Noller. 1994. Selective perturbation of G530 of 16 S rRNA by translational miscoding agents and a streptomycin-dependence mutation in protein S12. *J. Mol. Biol.* 235:156–172.

58. O'Connor, M. O., and A. E. Dahlberg. 1995. The involvement of two distinct regions of 23 S ribosomal RNA in tRNA selection. *J. Mol. Biol.* 254:838–847.

59. Ban, N., P. Nissen, …, T. A. Steitz. 1999. Placement of protein and RNA structures into a 5 Å-resolution map of the 50S ribosomal subunit. *Nature.* 400:841–847.

60. Kim, H. D., J. D. Puglisi, and S. Chu. 2007. Fluctuations of transfer RNAs between classical and hybrid states. *Biophys. J.* 93:3575–3582.

61. Uemura, S., M. Dorywalska, …, S. Chu. 2007. Peptide bond formation destabilizes Shine-Dalgarno interaction on the ribosome. *Nature.* 446:454–457.